Large-Eddy Simulations of wind turbine wakes in sheared inflows

Anand Parinam, Pierre Bénard, Dominic Von Terzi, Axelle Viré

Large-Eddy Simulations of wind turbine wakes in sheared inflows

Anand Parinam[1,2], Pierre Benard[2], Dominic von Terzi[1] and Axelle Viré[1]

[1] Faculty of Aerospace Engineering, Delft University of Technology, The Netherlands
[2] CORIA, CNRS UMR6614, Normandie Université, INSA and University of Rouen, 76801 Saint-Etienne-du-Rouvray, France.

E-mail: A.parinam@tudelft.nl

Abstract. Modern-day wind turbines are growing continuously in size and reach diameters of more than 200 m in an effort to meet the fast growing demand for wind energy. As a consequence, the rotors are exposed to larger velocity variations in the approach flow due to the presence of shear, veer and turbulence. The shear of the ambient flow is an important effect that can impact the wake of a turbine twofold: one way is how the wake evolves in the sheared flow; the other way is by impacting the performance and loading of the turbine and, hence, the wake it produces. Both ways can affect the size, shape, spreading and recovery of the turbine wake and, consequently, impact on loads and power output of turbines located downstream. In this study, we analyzed the influence of different inflow wind shear configurations on the evolution of the wake behind the IEA 15MW reference wind turbine by means of high-resolution Large-Eddy Simulations. In order to isolate the shear effects, the mean and hub height wind speed of the inflow was kept constant by prescribing linear shear profiles without turbulence. The influence of Coriolis forces and thermal stratification are neglected. In addition, the effect of the imposed shear on the turbine's power and thrust, and the effect of including the nacelle in the simulation, were monitored.

1. Introduction

The increasing energy demand and decreasing cost of renewable electricity sources, like wind and solar energy, over the past years has spurred an impressive growth of their deployment. To meet the growing demand, wind turbines are getting larger in size and in rating, exceeding rotor diameters of 200 m. The overall performance of these giant turbines varies significantly in the diurnal cycle marked by the presence of different atmospheric conditions [1, 2]. Therefore, the behavior of flow fields around wind turbines caused by various atmospheric conditions needs to be understood well to accurately predict performance and efficiently operate wind farms and turbines [3].

In particular under stable conditions, with high shear and low turbulence [4], turbine wakes persist farther than under often studied neutral conditions and, hence, more severely impact waked turbines downstream. The (high) shear can impact the wake of a turbine twofold. One way is how the wake evolves in the sheared flow, i.e. how the large flow structures that are responsible for mixing and energizing the wake are convected and grow in size or decay to small-scale turbulence. The other way is by impacting the performance and loading of the

turbine and, hence, how the wake is produced. Both ways can affect the size, shape, spreading and recovery of the turbine wake and, consequently, impact on loads and power output of waked turbines. Due to the significant wind shear and turbulence occurring in the atmospheric boundary layer (ABL), the response of wind turbines to such flow conditions has been examined to some extent [5, 6, 7, 8].

Wind turbine wakes comprise of a large number of temporal and spatial structures that are created in the region of velocity-deficit downstream of the wind turbine, generated by the blade rotation [9]. Hodgkin et al. [10] showed that shear has a significant impact on the evolution of the tip vortices and, therefore, on the shape of the wake, whereas thermal stratification only affects the near-wake region. In the literature, it was also shown that the presence of wind shear can produce a highly complex wake structure downstream of the turbine rotor that exhibits significant asymmetries, streamwise vorticity generation, non-periodicity, and non-uniformity [11]. In wind farms, the interaction of turbine rotors with this complex wake flow field may generate significant unsteady loading on blade structures. The power losses due to wake effects also can be quite significant [12]. To anticipate aerodynamic performance and structural loads, the wake zone must be accurately analyzed under various free-stream conditions.

This paper focuses on the study of the physics governing the behavior of wakes from large wind turbines, like the IEA 15MW reference design [13], for both the near and far wake regions under the influence of wind shear. Large-Eddy Simulations (LES) are used to accomplish this exploration. In order to isolate the shear effects, the mean and hub height wind speed of the inflow was kept constant by prescribing linear shear profiles without turbulence. The influence of Coriolis forces and thermal stratification are neglected. The paper is organized as follows. Section 2 reviews the methodology comprising of the governing equations and test case configuration. Section 3 presents the results of the influence of wind shear on the performance of the turbine and on the wake structure. Finally, Section 4 summarizes the main findings and draws conclusions.

2. Methodology

2.1. Governing equations

LES of flow past a single three-bladed turbine is carried out using the YALES2 massively parallel platform [14]. It solves the three-dimensional incompressible filtered Navier-Stokes equations with 4th-order time and space integration schemes:

$$\frac{\partial(\widetilde{u}_j)}{\partial x_j} = 0 \tag{1}$$

$$\frac{\partial}{\partial t}(\widetilde{u}_i) + \frac{\partial}{\partial x_j}(\widetilde{\widetilde{u}_i\widetilde{u}_j}) = -\frac{\partial}{\partial x_i}(\frac{\widetilde{p}}{\rho} + \frac{2}{3}k_{\text{sgs}}\delta_{ij}) + \frac{\partial\widetilde{\tau}_{ji}}{\partial x_j} - \frac{\partial}{\partial x_j}(2\rho\nu_{sgs}\widetilde{S^*_{ij}}) + F_p \tag{2}$$

where $\widetilde{u}_i$ is the filtered velocity field, $\widetilde{p}$ the filtered pressure field, ν_{sgs} is the sub-grid scale kinematic viscosity, $\widetilde{S^*_{ij}}$ is the strain rate tensor, and k_{sgs} is the kinetic energy of sub-grid scales. As we do not use a model for k_{sgs}, a modified pressure of $\widetilde{p} + \frac{2}{3}\rho k_{\text{sgs}}$ is computed instead. In this work, ν_{sgs} is modeled according to the Smagorinsky model [15]. The body force F_p in Eq. 2 represents the effect of the wind turbine on the flow. This term is modeled by using the Actuator Line Method (ALM) [16]. As such, each rotor blade is represented by a line discretized by points on which a space-time point force, $f_{N,m}$, is computed. The indices N and m denote the blade number and the position along that blade, respectively. The force values are computed based on the local flow field at the points and the associated airfoil lift and drag coefficients. This force is then projected onto the Eulerian grid cells of the surrounding flow field by using a Gaussian kernel function $\eta_{N,m}$ [17], i.e.

$$F_p(x_p, y_p, z_p, t) = -\sum_N \sum_m f_{N,m}(x_{N,m}, y_{N,m}, z_{N,m}, t)\eta_{N,m}\,, \tag{3}$$

$$\eta_{N,m} = \frac{1}{\epsilon^3 \pi^{3/2}} \exp\left[-\left(\frac{r}{\epsilon}\right)^2\right], \tag{4}$$

where ϵ denotes the mollification parameter that controls the kernel's width.

2.2. Configuration

This work uses the IEA 15MW reference wind turbine [13], a large and academic three-bladed turbine representative of state-of-the-art offshore machines. As represented in Figure 1, the turbine rotor of diameter D is placed at $3D$ downstream of the inlet and at mid-height and mid-span of the computational domain with size $6D \times 6D \times 20D$. An unstructured mesh with refinement near the turbine is used where the cell size is $\Delta x = 1.96\,\text{m} = 0.00816D$ accounting for a total of around 520 million tetrahedra. A preliminary mesh refinement study performed on both IEA 15MW and NREL 5MW turbines showed that the effect of grid refinement did not significantly affect the mean velocities but had a strong impact on the vorticity and wake structure. Therefore, the finest mesh of the grid refinement study was chosen for this analysis. The rotor blades are discretized in the spanwise direction into 64 points and the smearing factor is defined as $\epsilon/\Delta x = 2$.

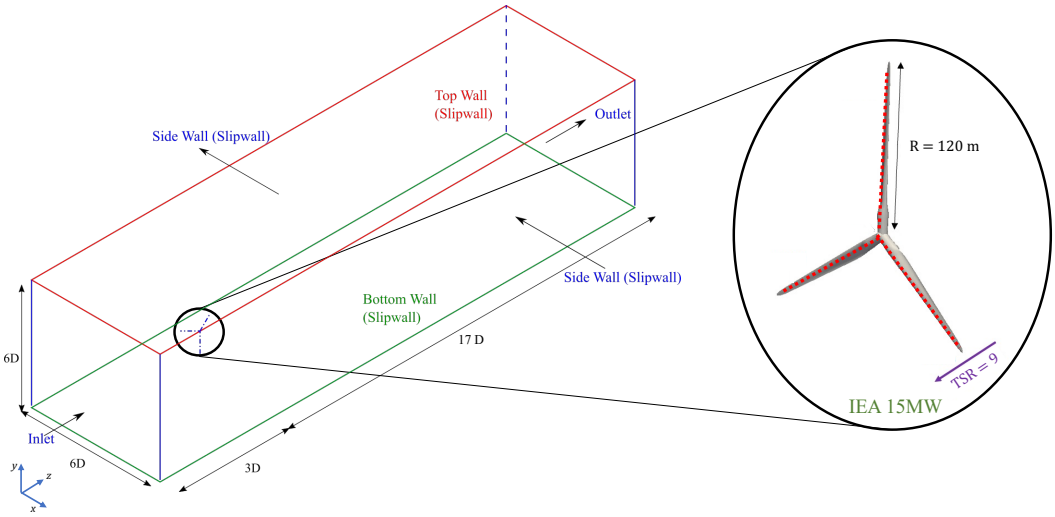

Figure 1: Schematic of the computational domain (adapted from [18, 19]).

3. Results

In order to assess the need for a nacelle in the numerical set-up, a preliminary study of the turbine wake with and without nacelle is first performed in Section 3.1. Then, the effect of wind shear on the wake structure is analysed in Section 3.2.

3.1. Effect of nacelle

The influence of the turbine nacelle on the wake characteristics is first investigated as a preliminary study on the NREL 5MW turbine with same set-up conditions and mesh resolution $\Delta x/D$ as presented before. The nacelle is approximated as a cylinder using the Brinkmann penalization technique [20], a classical Immersed Boundary Method. This penalization function

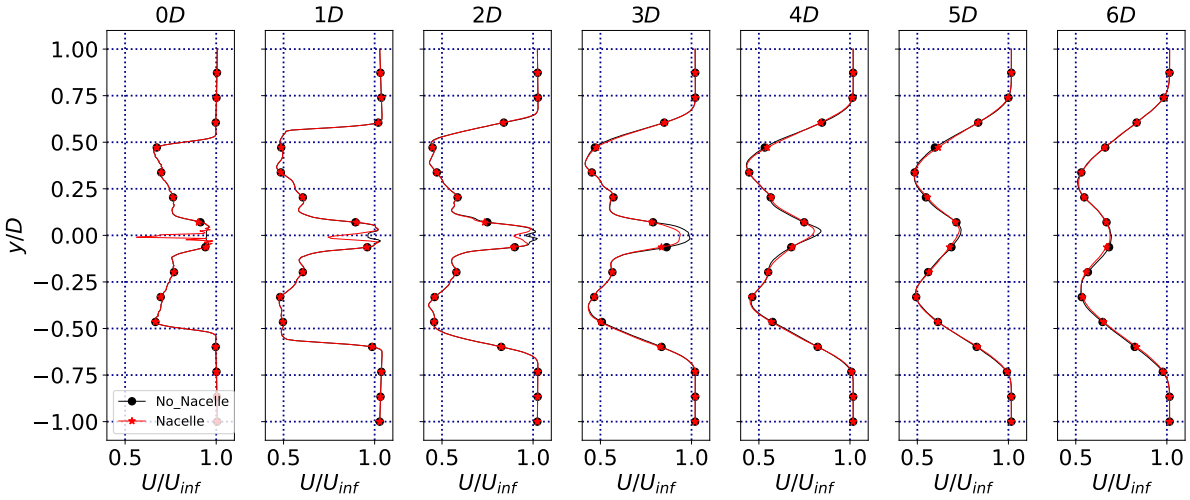

Figure 2: Mean streamwise normalised velocity profiles at different axial positions with (red star) and without (black dot) nacelle.

imposes a forcing term causing a zero-velocity field inside the nacelle. The rotor-nacelle setup is subjected to a uniform non-turbulent inflow without shear. The influence of the tower is here neglected due to the simplified atmospheric inflow set-up.

Mean streamwise normalised velocity profiles at different axial positions, with and without nacelle, are shown in Figure 2. In the absence of the nacelle, the flow accelerates at the hub center. By contrast, in the presence of the nacelle, the flow is blocked completely. However, this blockage does not affect the velocity profiles at distances larger than $1D$ from the hub region. Additionally, the impact of the nacelle decreases as the distance from the rotor increases and becomes insignificant beyond $2D$ away from the rotor. In the far-wake, beyond $4D$ from the rotor, there is no significant difference in the mean velocity profiles with and without nacelle. Similar analyses were performed on root-mean-square (r.m.s.) velocities in the streamwise locations as well as the streamwise velocity in x-normal planes, but are not shown here for the sake of brevity. For both cases, r.m.s. turbulent velocities were found to be in the same order with minimal impact of the nacelle on their values. The x-normal velocity planes show that the nacelle's influence is dominated by the turbulent mixing of the flow. Based on this short analysis, it is assessed that the nacelle can be neglected when only the far wake is studied. It is, therefore, omitted in the rest of this paper.

3.2. Effect of wind shear

The main study of this work concerns the effect of shear on the wake. Simplified shear conditions are imposed via a uniform vertical velocity gradient at the inlet. This linear vertical velocity profile is presented in Eq. 5 whose slope is obtained using the well-known power law [21] for different wind shear coefficients. Here, u_{ref} is imposed as $8m/s$ at hub height of $150m$. The four cases chosen for analysis are explained in Table 1 and their corresponding results are explained hereafter.

$$u = u_{ref} * (1 + \alpha \frac{y}{h_{ref}}) \tag{5}$$

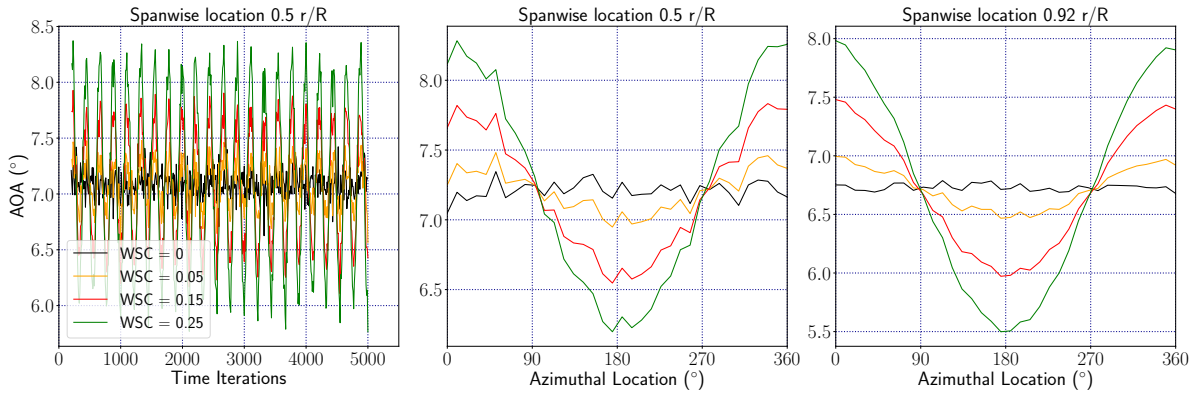

Figure 3: Variation of angle of attack with blade rotation and time iterations.

3.2.1. Turbine performance The velocity variations caused by shear across the rotor has two major consequences. One is that, due to power scaling with U^3, higher shear can lead to an increase in power (see Table 1). On the other hand, as the IEA 15MW uses collective pitch control, the shear will also cause angle of attack (AoA) variations as the blade rotates through the shear. This is shown in Figure 3. On the left, a time series of the angle of attack at a mid-span location of the blade is shown. A phase average of the same data (see center plot), clearly identifies the increase of AoA variations with shear. The same behavior is also shown in Figure 3, on the right, for an outboard blade section that is more relevant for the power production. These AoA variations result in operating the corresponding airfoils further away from their design point. As a consequence, the rotor will produce less power. For small shear, the second effect dominates (see Table 1), while for larger shear the first effect wins, as long as the AoA for stall is not reached. Similarly, the thrust of the turbine is affected (see Table 1). Bear in mind that, in particular for the lower shear cases, these variations in power and thrust are rather small and, in particular for power, would be a challenge to measure in the field. In line with the above reasoning, the behaviour of average power tends to increase with increasing shear. The maximum power is found for the highest shear conditions with a 1.6% increase. The behaviour of average thrust of the rotor first decreases slightly and then increases slightly with increasing shear. Due to this small variation in thrust and operating at the same rotation rate of the rotor, we can expect a very similar wake being produced across the shear values considered in this work.

Table 1: Tip vortex behavior based classification of (near) wake regions for different wind shears and impact of shear on turbine performance.

Test Case	Linear Region	Transition Region	Turbulent Region	Change in Power [%]	Change in Thrust [%]
WSC = 0	0D - 1.5D	1.5D - 4.5D	4.5D	-	-
WSC = 0.05	0D - 1.5D	1.5D - 4D	4D	- 0.01	- 0.02
WSC = 0.15	0D - 1.2D	1.2D - 3.5D	3.5D	0.29	-0.05
WSC = 0.25	0D - 1D	1D - 3D	3D	1.62	0.20

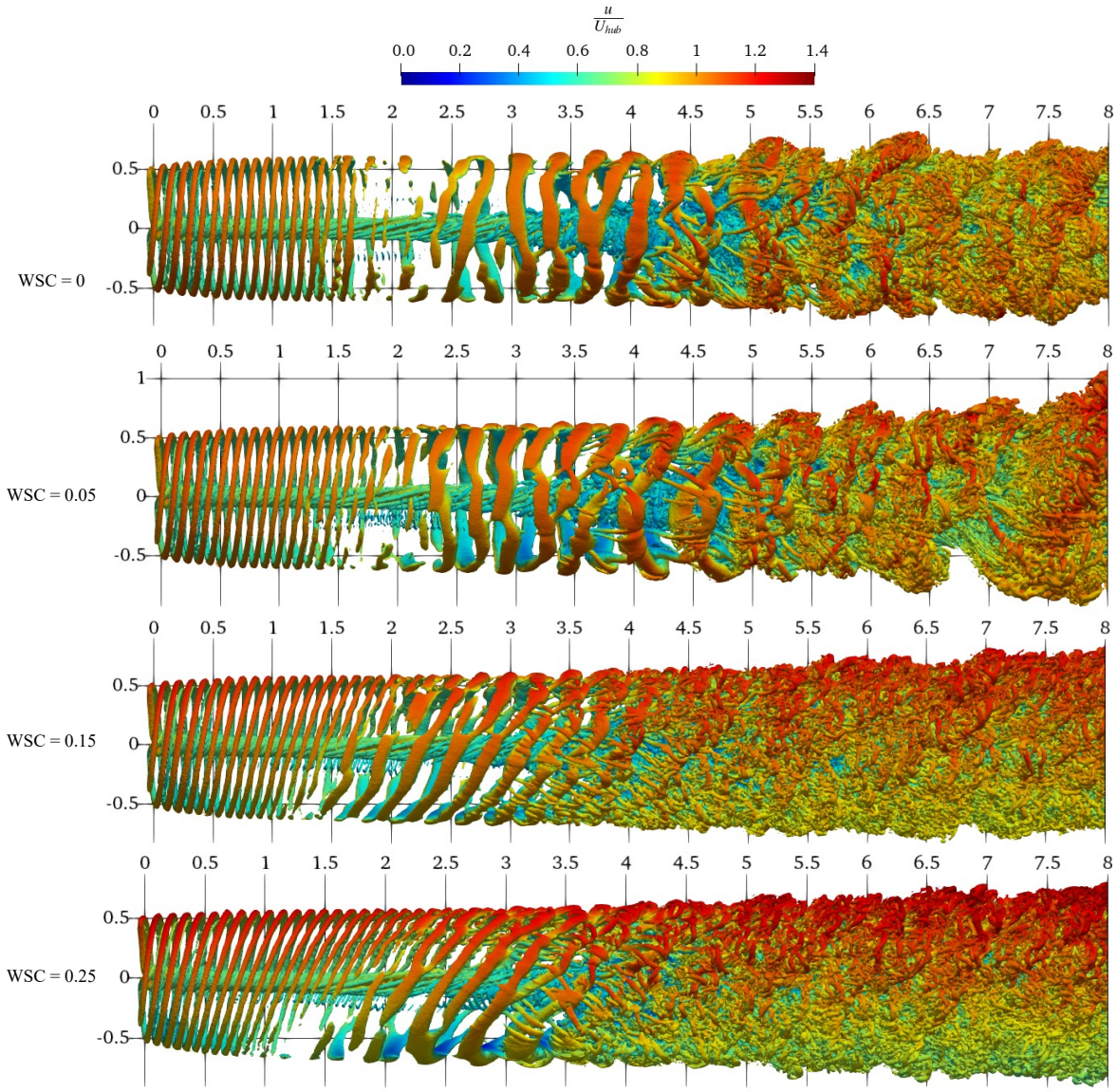

Figure 4: Iso-contours of Q-Criterion for iso-value of $0.001\,\mathrm{s}^{-2}$, coloured by the non-dimensional velocity magnitude, for different wind shear coefficients from WSC=0 (top) to WSC=0.25 (bottom).

3.2.2. Wake structure Figure 4 shows iso-contours of the Q-Criterion for an iso-value of $0.001\,\mathrm{s}^{-2}$ coloured by the non-dimensional flow speed, for different values of the shear coefficient, i.e. from no shear to a wind shear coefficient (WSC) of 0.25. As can be expected, higher shear causes the helical tip vortices to convect more quickly at the top than at the bottom resulting in a tilting of this flow structure. A proper orthogonal decomposition (POD) analysis, as performed by Hodgkin et al. [10] for a wind turbine in shear and explained in [22], would show that the tip vortices can be identified as the dominant helical mode with an associated frequency and wavelength. In Fig. 4, this wavelength can be discerned as the distance between the visible vortex lines. It is also known as the streamwise vortex separation distance. For all cases, this distance increases a few diameters downstream of the wind turbine, i.e., in a POD analysis, a different mode with a larger wavelength and a lower frequency has become dominant while the

helical mode visible upstream has decayed. For higher shear, this situation occurs earlier at the slower bottom and later at the faster top.

The near-wake structure can be classified in three regions: linear, transition and turbulent based on the tip vortex behavior described above and as proposed in [10]. Note that, in our work, the classification is based only on visual inspection over a range of iso-surfaces. A more robust way would have been to perform a suitable decomposition technique like POD as explained in [22] and used in [10]. Note also that we focus on the tip vortices as the largest flow structures in the wake that are presumably providing the bulk of the mixing and, hence, likely contribute strongest to the wake recovery. We will look at statistical quantities of the full wake below. The linear region reaches from the hub to as long as the increase in strength of the tip vortices could be described with Linear Stability Theory. For the analysis here, we take the location where roughly the first change in dominant helical structures occurs, i.e. a change in observed spacing. Strictly speaking, the linear region will have been exceeded by then, but it will be within the accuracy of how we determine it (i.e. within $0.5D$). The linear region is followed by the transition region, which extends until the zone where the tip vortices break down into smaller ones. The size of each region of this classification is presented in Table 1 for each of the four shear values α considered here.

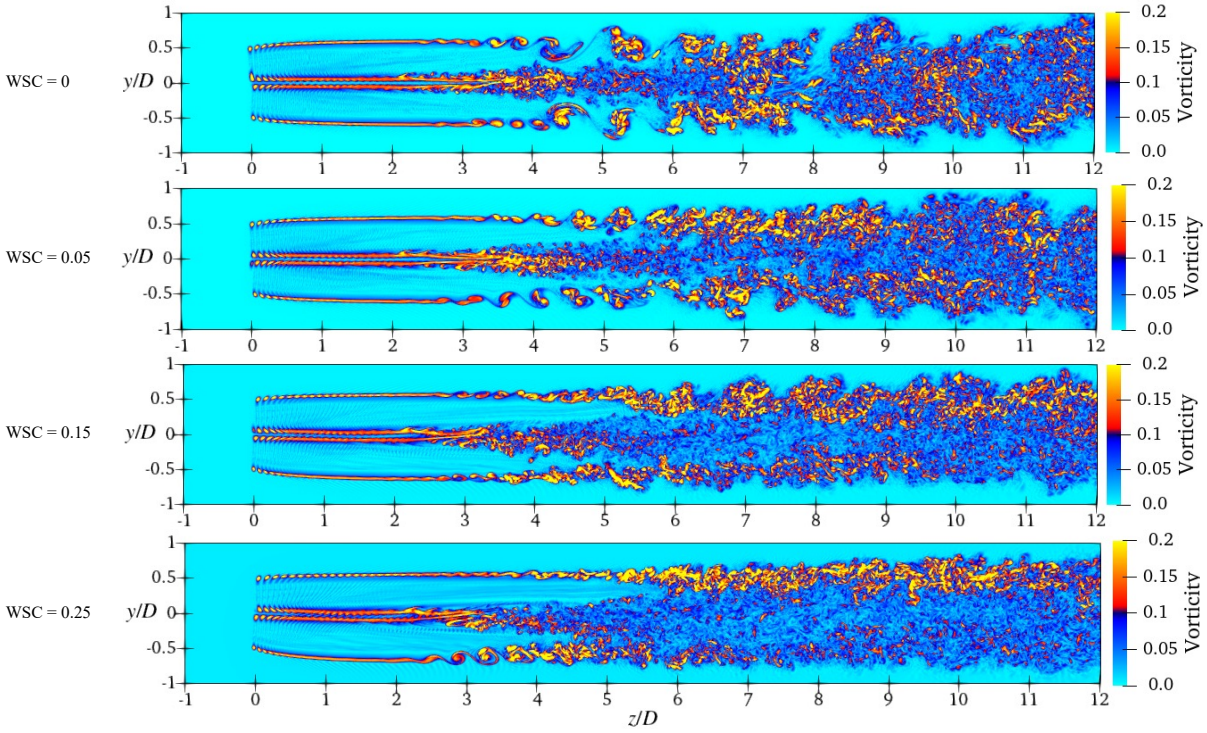

Figure 5: Streamwise vorticity contours in a x-plane for different wind shear coefficients, from WSC=0 (top) to WSC=0.25 (bottom).

Under the effect of sheared inflow, the linear region is shortened as the vortical structures are elongated at the top and stretched at the bottom. As indicated in Table 1, this first region extends to $1.5D$ (without shear) and to $1D$ (with $WSC = 0.25$). Similar trends can be observed in the transition and turbulent regions. The transition to the intermediate region depends on the stability of helical structures as well as the spacing between them. The initial spacing is,

for all shear values, similar to the ones without shear. This suggests that the same tip vortices are produced, which is consistent with the conclusion from Section 3.2.1, that suggests a weak influence of change in turbine operation with shear due to AOA variations. From this, one can support the common notion that the shortening of the regions are due to an increased instability of the tip vortices with increase in shear.

Figure 5 represents the vorticity magnitude for different shear coefficients on the mid-span x-normal plane. The increase in wind shear coefficient causes the tip vortices to roll up and "pair" more quickly, i.e. to increase their spacing. Also the breakdown to turbulence occurs further upstream. This is consistent with the findings from before. The vorticity level distribution also shows a dichotomy between low and high shears. With low shear, the vorticity levels are similar between the top and bottom streams. In contrast, the vorticity levels are higher in top streams compared to bottom streams for higher sheared inflow. This may hint to less mixing overall, an observation we will pick up on below.

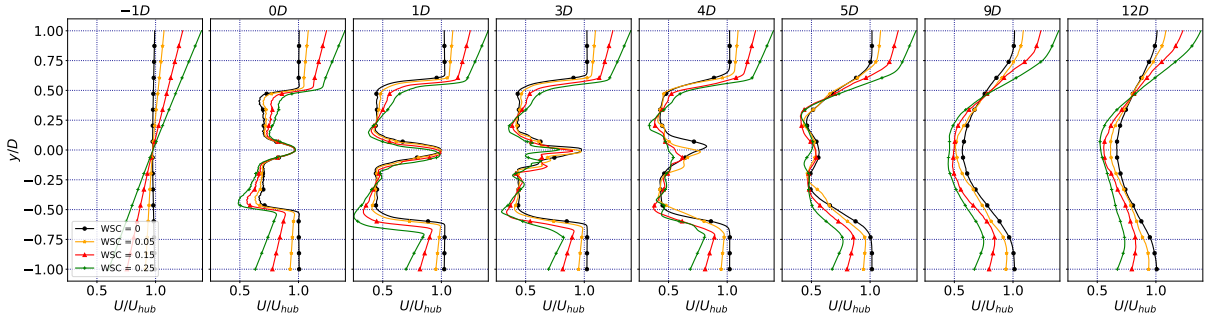

Figure 6: Mean streamwise normalised velocity profiles in a x-plane for different wind shear coefficients, from WSC=0 (top) to WSC=0.25 (bottom).

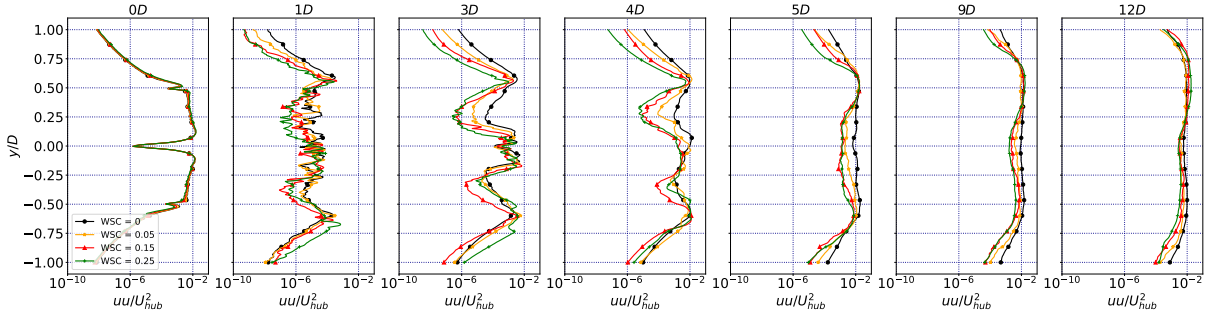

Figure 7: Variance of streamwise normalised velocity profiles in a x-plane for different wind shear coefficients, from WSC=0 (top) to WSC=0.25 (bottom).

3.2.3. Velocity distributions Figures 6 and 7 present the evolution of the flow over different upstream and downstream locations of the rotor plane in the streamwise directions using the profiles of time-averaged and r.m.s. velocities. The averaging has been performed over 350 blade rotations. The profiles at $x = -1D$ show the initial undisturbed velocity profiles for different WSC at the inlet of the rotor. The effect of wind shear on the rotor can be clearly seen from $0D$ to $3D$ downstream of the rotor. Since the flow follows a linear shear, the velocities at the

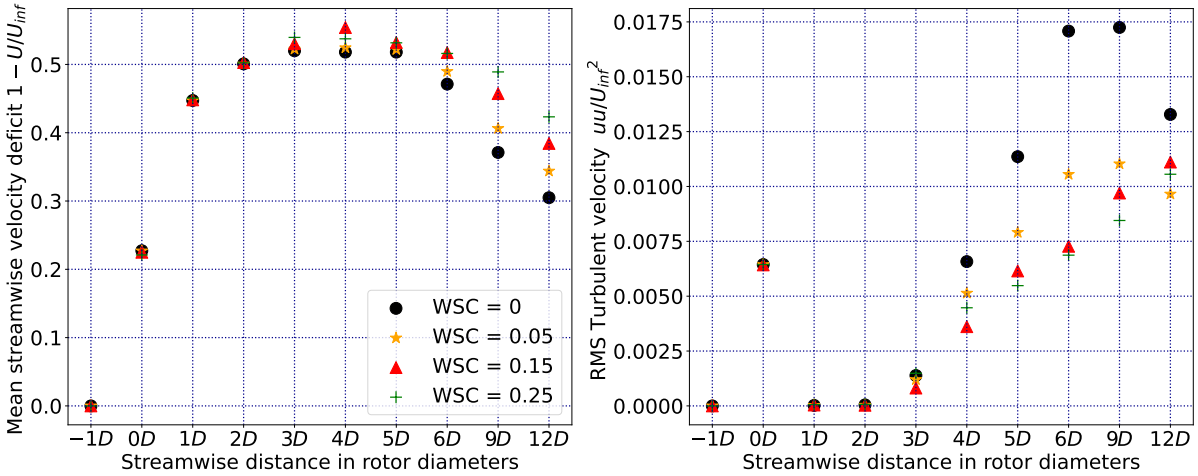

Figure 8: Integrals of mean streamwise normalised velocity deficits (left) and variance of streamwise normalised velocities (right) in a x-normal plane for different wind shear coefficients.

top of the rotor are higher compared to the bottom of the rotor and this effect scales linearly with increasing WSC.

At roughly $4D$ downstream, the wake recovery process starts. Since the inflow is non-turbulent, the variance of velocities have a low level from $-1D$ to $4D$. Beyond $5D$, breaking down of large-scale structures into smaller structures following the turbulent kinetic energy cascade leads to the increase of turbulence in the flow and, consequently, of the velocity fluctuations.

Figure 8 gathers the integral of the mean velocity deficit and the integral of the variance of velocities at different axial locations. The mean integral shows the wake recovery, whereas the integral of the variance of velocities is a measure of the turbulence in the whole wake. This needs to be distinguished from the local turbulence due to the tip vortex breakdown. The velocity deficit first increases and reaches a peak at around $4D$ to $5D$. From here the wake recovery starts and, hence, the deficit gradually decreases for all wind shears. In the near-wake region, the velocity deficits are similar for all the values of shear coefficients. In contrast, in the far-wake region, around $6D$ to $12D$, the velocity deficit is larger for higher shear. Lower velocity deficits imply more mixing in the flow. Note that the turbulence levels in the whole wake, as indicated the integral of variance of streamwise velocity, is lower for higher shear, further indicating a lower mixing for higher levels of shear in the inflow.

4. Conclusions

We performed high-resolution LES of the wake generated by the IEA 15MW reference wind turbine in sheared inflow. The turbine was modeled using the ALM method. To isolate the impact of shear on the on the near- and far-wake characteristics, linear shear profiles without turbulence were imposed at the inflow such that mean and hub height wind speeds were identical. Moreover, the influence of Coriolis forces and thermal stratification were neglected. A preliminary study showed that taking the nacelle into account was not needed for the purpose of this investigation. Due to operation in shear, it was shown that, as expected, increasing AOA variations for increasing inflow shear occurred. However, it was concluded, that the dominant effect on power was due to its scaling with the square of the wind speed. On the other hand, thrust variations were small. The latter together with analysing the near wake behavior showed that the wakes produced were quite similar in all the shear cases and the study is likely to indeed show the evolution of the wake due to its exposure to shear.

The simulations showed that, for higher shear values, the tip vortices in the near-wake tilted with the shear and rolled up, paired and broke down to small scales quicker. On the other hand, in the far wake, higher shear resulted in a reduction in wake recovery and a lower turbulence intensity in the wake as a whole. This is consistent with the common observation that, in the stable atmospheric boundary layer of higher shear and lower turbulence, the wake deficit reaches farther downstream resulting in a larger power loss of waked turbines downstream. This suggests that the local small-scale structures near the tip are less effective in transporting high-momentum fluid to the wake core in order to promote the wake recovery.

A consequence of the findings from the present study is that wake control methods, that try to accelerate the breakdown of tip vortices, should be tested in stable atmospheric conditions. This is necessary, as they may lead to an undesired reduction in mixing that will be not (or much less) observed for neutral and unstable stability conditions. To verify this hypothesis, a consistent manipulation of the tip vortices, similar to the approach developed in [23], could be used. In addition, other effects of the stable boundary layer, like veer and the presence of (low) turbulence in the approach flow should be included in any follow up study of the work presented here.

Acknowledgments
The authors are grateful to SURF for the computational time made available on the Dutch national supercomputer Snellius (grant number : EINF-4231). Simulations were alsoperformed using DelftBlue [24] at TU Delft, HPC/AI resources of TGCC under the allocation 2022-A0102A11335 made by GENCI, and CRIANN resources under the allocation 2012006. This research has been supported jointly by TU Delft and Région Normandy in France.

References

[1] Calaf M, Meneveau C and Meyers J 2010 *Physics of Fluids* **22** 015110
[2] Rodrigo J S, Arroyo R A C, Moriarty P, Churchfield M, Kosović B, Réthoré P, Hansen K S, Hahmann A and and J D M 2017 *Wiley Interdisciplinary Reviews: Energy and Environment* **6**
[3] Veers P, Dykes K, Lantz E, Barth S, Bottasso C and et al 2019 *Science* **366**
[4] Abkar M, Sharifi A and Porté-Agel F 2016 *Journal of Turbulence* **17** 420–441
[5] Park J, Basu S and Manuel L 2014 *Wind Energy* **17** 359–384
[6] Gadde S N and Stevens R J A M 2021 *Phys. Rev. Fluids* **6**(1) 014603
[7] Strickland J M, Gadde S N and Stevens R J 2022 *Renewable Energy* **197** 50–58
[8] Chanprasert W, Sharma R, Cater J and Norris S 2022 *Renewable Energy* **201** 1096–1110 ISSN 0960-1481
[9] Uchida T 2020 *Energies* **13** 1–31
[10] Hodgkin A, Laizet S and Deskos G 2022 *Journal of Physics: Conference Series* **2265** 022061
[11] Sezer-Uzol N and Uzol O 2013 *Wind Energy* **16** 1–17
[12] Hansen K S, Barthelmie R J, Jensen L E and Sommer A *Wind Energy* **15** 183–196
[13] Gaertner E, Rinker J, Sethuraman L, Zahle F and et al 2020 *NREL/TP-75698*
[14] Moureau V, Domingo P and Vervisch L 2011 *Comptes Rendus Mécanique* **339** 141–148 ISSN 1631-0721 high Performance Computing
[15] Smagorinsky J 1963 *Monthly Weather Review* **91**
[16] Sorensen J N and Shen W Z 2002 *Journal of Fluids Engineering* **124** 393–399 ISSN 0098-2202
[17] Jha P, Churchfield M, Moriarty P and Schmitz S *Accuracy of State-of-the-Art Actuator-Line Modeling for Wind Turbine Wakes*
[18] Schmitz S and Jha P K 2013 *Annual Forum Proceedings - AHS International* **3** 2228–2235
[19] Ravensbergen M, Bayram Mohamed A and Korobenko A 2020 *Computers Fluids* **201** 104465 ISSN 0045-7930
[20] Kevlahan N K R and Ghidaglia J M 2001 *European Journal of Mechanics - B/Fluids* **20** 333–350 ISSN 0997-7546
[21] Emeis S and Turk M 2007 *Wind Energy* 61–64
[22] von Terzi D, Sandberg R and Fasel H 2009 *Computers & Fluids* **38** 1638–1650
[23] Schneider H, von Terzi D, Rodi W and Bauer H J 2011 *Journal of Fluid Mechanics* **687** 584–594
[24] Delft High Performance Computing Centre (DHPC) 2022 DelftBlue Supercomputer (Phase 1) `https://www.tudelft.nl/dhpc/ark:/44463/DelftBluePhase1`